9-28-2022

Image Processing in Dense Forest Areas using Unmanned Aerial System (UAS)

Parth Bhatt
Michigan Technological University, ppbhatt@mtu.edu

Curtis Edson
United States Air Force Academy

Ann Maclean
Michigan Technological University, amaclean@mtu.edu

APPLICATIONS-WHITE PAPER

Image Processing in Dense Forest Areas using Unmanned Aerial System (UAS)

Authors: Parth Bhatt[1], Curtis Edson[2], Ann Maclean[1]

Affiliations: [1]College of Forest Resources and Environmental Science, Michigan Technological University, [2]Department of Economics and Geosciences, United States Air Force Academy

Description: A detailed workflow using Structure from Motion (SfM) techniques for processing high-resolution Unmanned Aerial System (UAS) NIR and RGB imagery in a dense forest environment where obtaining control points is difficult due to limited access and safety issues.

Abstract: Imagery collected via Unmanned Aerial System (UAS) platforms has become popular in recent years due to improvements in a Digital Single-Lens Reflex (DSLR) camera (centimeter and sub-centimeter), lower operation costs as compared to human piloted aircraft, and the ability to collect data over areas with limited ground access. Many different application (e.g., forestry, agriculture, geology, archaeology) are already using and utilizing the advantages of UAS data. Although, there are numerous UAS image processing workflows, for each application the approach can be different. In this study, we developed a processing workflow of UAS imagery collected in a dense forest (e.g., coniferous/deciduous forest and contiguous wetlands) area allowing users to process large datasets with acceptable mosaicking and georeferencing errors. Imagery was acquired with near-infrared (NIR) and red, green, blue (RGB) cameras with no

ground control points. Image quality of two different UAS collection platforms were observed. Agisoft Metashape, a photogrammetric suite, which uses SfM (Structure from Motion) techniques, was used to process the imagery. The results showed that an UAS having a consumer grade Global Navigation Satellite System (GNSS) onboard had better image alignment than an UAS with lower quality GNSS.

1. Introduction

Unmanned Aircraft Systems (UAS), or Unmanned Aerial Vehicle (UAV), are a rapidly emerging image acquisition technology. The US Department of Defense (DoD, 2019) and Civil Aviation Authority (CAA, 2015) of the UK adopted the term UAS. The term Remotely Piloted Aerial System (RPAS,) a particular type of UAS, was introduced by the International Civil Aviation Authority (ICAO) in ICAO Circular 328 (ICAO, 2011). According to a recent market research study (Markets, 2018) the global UAS market was $18.14 billion in 2017 and is projected to reach $52.30 billion by 2025. High spatial and temporal resolutions are two important characteristics of UAS. Other factors such as low-cost, smaller components size, longer battery life, improved launching capabilities, and ease of transport and operation make this a preferable choice over other remote sensing platforms for various applications.

The Federal Aviation Administration (FAA) categorizes a UAS as weighing under <=23 kg (55 lbs) as small Unmanned Aircraft Systems (sUAS) (FAA, 2018). Rango et al. (2009) states how small (55 lbs or <50 kg) and micro (11 lbs or <5 kg) UAS platforms provide many benefits for remote sensing applications over larger sized UASs. UASs

were used initially for various military purposes from data collection to strategic planning (Watts et al., 2012). The US National Aeronautics and Space Administration (NASA), under the "Mini-Sniffer" program, developed unmanned aircraft for atmospheric sampling during the 1970 - 80 (NASA, 2017). In the 1990s, NASA's Environmental Research Aircraft and Sensor Technology (ERAST) program highlighted the development and capabilities of UAS for various scientific research areas (NASA, 2008).

There are numerous studies available in the literature where researchers are using high-resolution satellite or manned aircraft imagery (i.e., NAIP, WorldView, Hyperspectral) to map forests (Hayes et al., 2014), urban landscape, wetlands (Berhane et al., 2018), community habitats mapping (Bhatt et al., 2022), disaster mapping (Bai et al., 2018) and surveillance (Casana & Panahipour, 2014), agriculture applications (Sidike et al., 2019), but the imagery from the private satellites can be expensive and temporal or spatial resolution for small study areas could be problematic (Adam et al., 2009). Similarly, UAS provides multiple civil applications including, but not limited to, long-term scientific research, high-spatial resolution aerial imagery, agricultural monitoring, pipeline surveillance, border protection, disaster management, weather monitoring and airborne communications (Bendig et al., 2014; Bhatt, 2018; Colomina & Molina, 2014; Gini et al., 2017) but not having the limitation of temporal or spatial resolution. The United States Geological Survey (USGS) has used UAS since 2010 for various research applications, ranging from monitoring shoreline erosion and rapid response volcano monitoring (Rango et al., 2009). Two types of UAS are widely available- fixed-wing and multi-rotor. Multi-rotors allow vertical take-off and landing with less open space, are

easier to maneuverer, and cost less. However, they have smaller areal coverage, shorter flying times, and are less durable in high winds (Cai et al., 2014; Thamm et al., 2015). Fixed-wing vehicles, are larger in size and more stable, cover larger areas and have a longer battery life. However, they require larger take-off and landing areas and are more expensive (Boon et al., 2017; Cai et al., 2014; Thamm et al., 2015).

Recently, using UAS imagery for mapping and classifying forest vegetation, wetlands delineation and invasive species monitoring has increased. Husson et al. (2014) used Personal Aerial Mapping System (PAMS) UAS imagery to interpret and delineate aquatic vegetation and *Phragmites* stands. Precision forestry practices have also increased the use of UAS for mapping forest cover types and stand conditions (Goodbody et al., 2017; Torresan et al., 2016). Dunford et al. (2009) used UAS image mosaics to characterize Mediterranean riparian forest. Dandois and Ellis (2013) illustrated the use of a lightweight, hobby grade UAS to map and observe 3D canopy phenology in temperate deciduous forest sites and incorporated structure from motion (SfM) algorithms in the image processing. Using a fixed wing UAS system to acquire high spatial resolution imagery (~7 cm) Getzin et al. (2012) assessed biodiversity by identifying canopy gaps in deciduous and deciduous-coniferous mixed forests in Germany; while Koh and Wich (2012) utilized lightweight fixed-wing drone in conservation efforts to survey and map forests and biodiversity. Carbonneau and Dietrich (2017) evaluated UAS data and utilized SfM (Structure from Motion) techniques for high-quality topography mapping.

Use of fixed-wing UAS with an on-board survey grade GPS operating in a ground control point (GCP) free environment was demonstrated by Chiang et al. (2012). Direct georeferencing using the SfM technique has been used successfully to process high spatial resolution imagery for agricultural areas requiring high locational accuracy (Cai et al., 2014; Turner et al., 2014). Others have shown the use of direct georeferencing without ground control points to process UAS imagery with survey grade GPS on-board (Eling et al., 2015; Gabrlik, 2015; Mian et al., 2015). Samiappan et al. (2016) mapped invasive *Phragmites australis* in coastal wetlands adjacent to the Gulf of Mexico using an Altavian Nova UAS platform with image spatial resolution as fine as 5 cm. In another study by Samiappan et al. (2016) in the Gulf of Mexico coastal wetlands, they used a hand launched Precision Hawk Lancaster UAS platform to acquire five band multispectral imagery with a high spatial resolution (~ 8 cm) to map *Phragmites* (common reed).

2. Study Area

The Hiawatha National Forest (HNF) is located in the central and eastern parts of Michigan's Upper Peninsula on the north coast of Lake Michigan (Figure 1), and manages the largest area of coastal wetlands in the Great Lakes Basin. HNF manages the greatest acreage of coastal wetlands in the Great Lakes Basin, encompassing 363,599 ha (898,472 ac) and over 161 km (100 miles) of Great Lakes shoreline, with jurisdiction along Lakes Michigan, Superior and Huron shorelines (US Forest Service, 2015). The study sites were selected for their diverse land-water vegetation communities including large tracts of forested, submergent, emergent, and shrub-scrub wetlands.

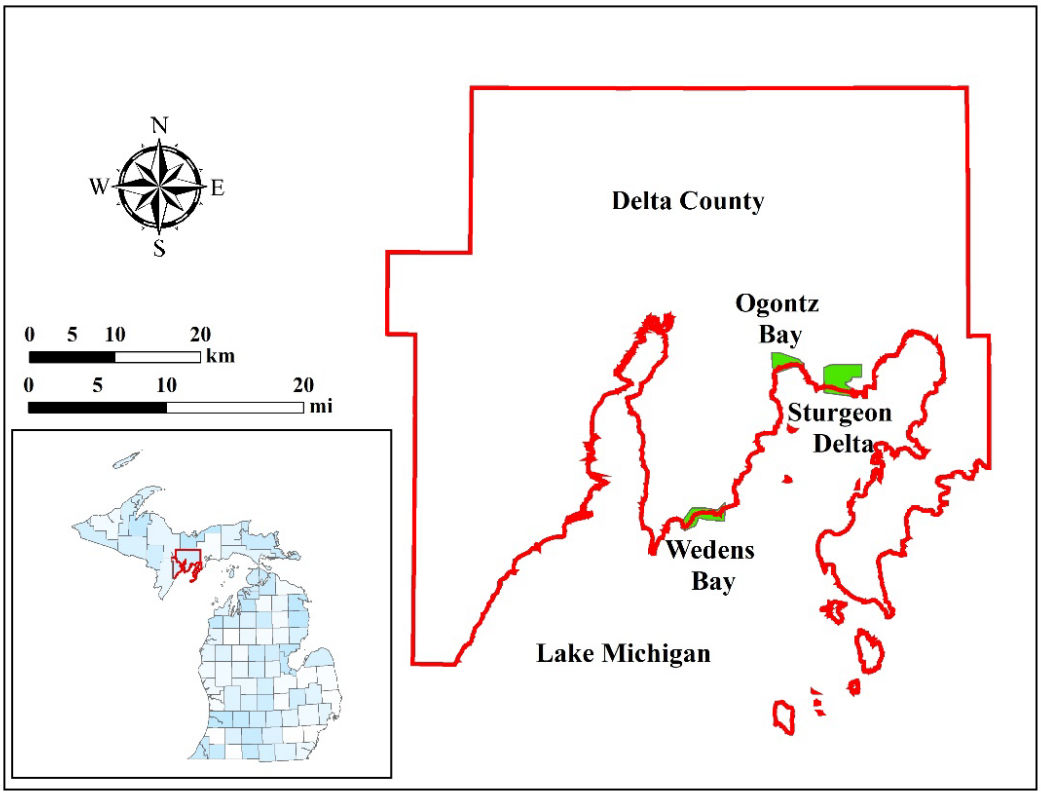

Figure 1. Location of the three UAS study sites in the Hiawatha National Forest in the central part of Michigan's Upper Peninsula along the Lake Michigan shoreline.

2.2 Objectives

There are few published UAS studies involving such a large 2,315 ha (5720.49 ac) study area. Most published studies deal with smaller areas focused on a particular plant species or agricultural crop. Dense forest stands, commonly found in the Upper Midwest, have limited accessibility due to remoteness and lack of roads/trails which severely curtails collecting GCPs. Hence, the objectives of this feasibility study were: to develop a rigorous processing workflow for a large UAS imagery dataset with few or no GCPs; and evaluate the capabilities of the fixed-wing UAS platform and data collection components.

3. Materials and Methods

Two UAS fixed wing platforms were utilized for the study. A Trimble (Trimble Inc., Sunnyvale, CA) UX5 and a UX5-HP. Both have an expanded polypropylene (EPP) foam fuselage, internal carbon frame, and a pusher propeller driven by an electric motor powered by lithium polymer (LiPo) battery. The Trimble UX5 was mounted with a low-cost mapping grade GNSS receiver located in the electronic control box (eBox), and a Sony a5100, 24-megapixel mirrorless camera with fixed 15mm lens capable of a ground sample distance (GSD) as fine as 2.0 cm and collected RGB imagery. The Trimble UX5-HP payload included a consumer grade GNSS receiver with dual frequency, eBox, and a Sony A7R, 36-megapixel mirrorless DSLR camera with a fixed 35mm lens and GSD capability of 1.0 cm and collected NIR imagery. A comparison of the UASs is compiled in Table 1 (Trimble, 2019b).

Table 1. Comparison of UAS devices used in the study (Trimble, 2019b).

Three areas (Figures 1 and 2) of coastal wetlands and adjacent interior wetlands were flown in August, 2017 with varying flying heights between 75 and 121 m (246-400 ft). Approximately 2,315 ha (5,720 ac) of imagery (~40,000 images) were acquired and collected over 52 flight blocks (Figure 2). The overlap and sidelap for all imagery were set to 80%. Project locations were on the Lake Michigan coastline, and taking off over water was relatively easy. However, both UASs require adequately sized, non-forested, dry, open space to land. Because the study sites were predominantly wetlands, lake levels high and few roads or trails, landing locations were limited.

Features	**UX5 HP**	**UX5**
Type	Fixed Wing, 100 cm (3.28 ft.) wingspan	Fixed Wing, 100 cm (3.28 ft.) wingspan
GNSS receiver	Dual-frequency L1/L2 GNSS (GPS, Glonass, Beidou, Galileo)	Lower grade GNSS
Camera type	Sony a7R, 36-megapixel, full frame, 35 mm lens, NIR camera	Sony a5100, 24-megapixel, 15 mm lens, RGB camera
Resolution	1.0 cm with 35 mm lens	2.0 cm with 15 mm lens
Weight	2.9 kg (6.4 lb)	2.5 kg (5.5 lb)
Battery	14.8 V, 6,600 mAh	6,600 mAh
Maximum flying speed	88 km/h (55 mph)	80 km/h (50 mph)
Maximum flying time	35 min	50 min

There were two batteries for the UX5 and four batteries for the UX5-HP, that were used singly, which is important for quick turn-around times for getting the UAS back in the air and collecting images. Manufacturer's estimated flight time capabilities were 50 and 35

minutes for the UX5 and UX5-HP respectively. This fell short when flying in the field, as preflight setup consumes ~ 10% of the battery life, and 10-15% battery life is required for safe landing. These reduced flight times necessitated careful consideration in flight planning and selecting landing sites.

A bungee cord catapult launched the aircraft to takeoff speed. Takeoff and landing locations were confirmed via the control tablet's internal GNSS receiver before takeoff. Most of the data collection was automated based on the programmed flight plan, which was communicated to the aircraft eBox via a FM modem. For flight mission planning and flight operations, Trimble's Aerial Imaging proprietary software designed for the Trimble UX5 series, was utilized. The software interfaces with Google Earth to download planning imagery for the study sites as shown in Figure 2.

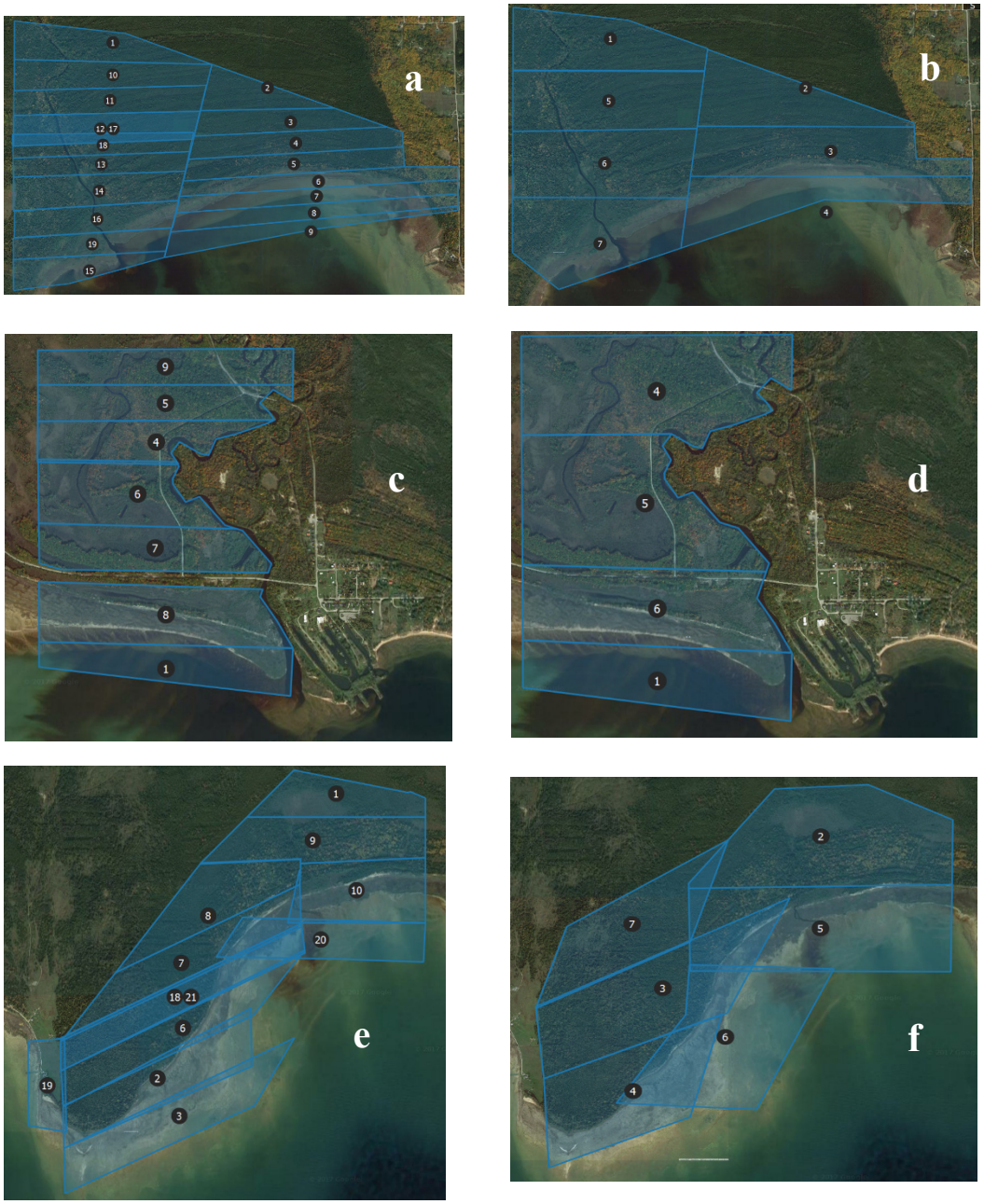

Figure 2. Number of blocks flown for collecting NIR and RGB data with Trimble UX5 HP and UX5 over the three study sites, Ogontz Bay-NIR (a), RGB (b), Sturgeon River Delta-NIR (c), RGB (d) and Wedens Bay-NIR (e), RGB (f). (Source: Google Earth, Aerial Imaging, Trimble).

Four flights per day were planned based on factors such as battery life, data download time for each flight, and preliminary office processing. Six was the maximum number of flights achieved in a day. Flight block planning size was based on actual battery life expectancy, with actual times of 45 minutes for the UX5 and 30 minutes for the UX5-HP. In many cases, acquisition of complete blocks was not possible due to strong winds coming off of Lake Michigan, which reduced flying times due to increased power and battery usage. Use of ground control targets for ground control points (GCPs) locations were not used due to inaccessibility caused by dense forest cover and lack of roads and trails.

3.1 Photogrammetric Processing

Initially, Trimble Business Center (TBC) and Trimble Inpho UASMaster (Trimble, 2019a) were used to process the data. However, large tracts of the coastal wetlands consisted of dense forest cover where accessibility and easily identifiable ground features did not exist (Figure 3). This precluded the software's automatic tie-point (ATP) algorithm from finding tie-points on overlapping photos; which in turn prevented or attenuated photo-mosaic creation and posed a serious image mosaicking issue (Hexagon, 2016). Manual tie-point location, often cited as an alternative approach, was not feasible due to the homogeneity of high-density forest cover and the large number of images (700 to 1,500 images) per block. Oblique views of different sides of the same trees make it very difficult and inordinately time consuming to identify the same feature (group of pixels).

Figure 3. Snapshot showing high-density forest cover across Sturgeon River Delta area. (RGB bands – UAS Imagery).

Deep-water areas of Lake Michigan also contributed to the problem, as the water was either relatively monochromatic with insufficient differentiation between pixels, or wind-driven wave action created different spectral reflectance in adjacent imagery for the same geographic location. To help troubleshoot alignment issues, the data were sent to Trimble Germany GmbH (Branch office Stuttgart; Rotebühlstraße 81; 70178 Stuttgart) and a team leader (Inpho Support - Imaging Division) assisted in the tie-point processing. After approximately three months of adjusting inputs and using various processing options, TBC and UASMaster were unable to adequately process the data, and it was concluded the software algorithms were not sufficient to process such highly dense forested areas (Figure 3).

Evaluation of the Agisoft Metashape (previously PhotoScan) Professional Edition Version 1.3, 2017 (Agisoft, 2017a) photogrammetry software package was initiated at the suggestion of USGS, National UAS Project Office (Sloan, 2017). Agisoft uses SfM algorithms (Agisoft, 2017b), and in a forested environment, achieved a higher percentage of success in photo alignment, generation of georeferenced point clouds, mesh creation and the resulting orthomosaic (Figure 4). SfM solves scene geometry, camera positions and internal and external orientation parameters using a bundle adjustment procedure, and automatically extracts features (matching points) from overlapping images. Metashape aligns photos without the use of GCPs. Input parameters used are based on software recommendations (Agisoft, 2017b), or if needed, by trial and error experimentation, to achieve acceptable results. The amount of processing time for each step, shown in Table 2, and the number of images processed during that time were based on the trial and error approach. The aircraft trajectory csv file, which contained photo station GNSS locations and image orientation parameters, as well as the imagery were imported imported into the software. Image quality was evaluated and assigned a value with 1 being the best. Values below 0.7 indicated the images had low contrast or vignetting effects and were discarded if area coverage was maintained by adjoining photos.

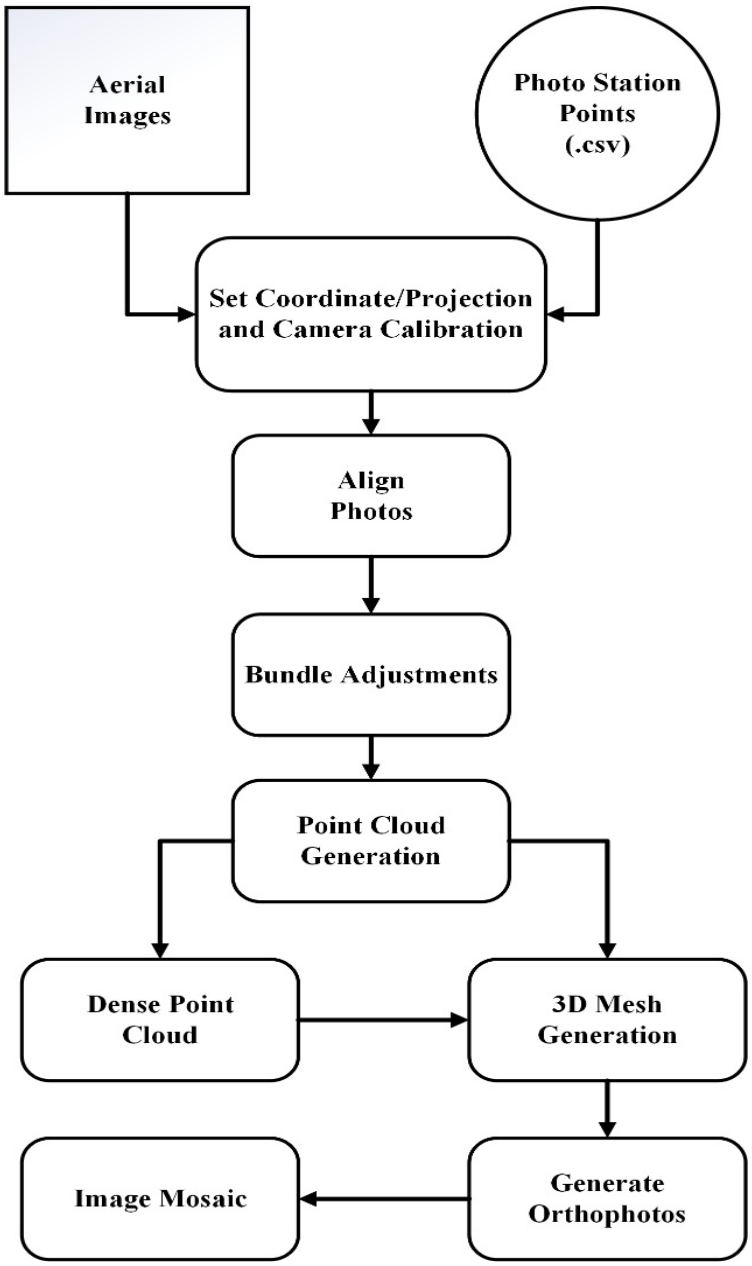

Figure 4. SfM workflow to process the UAS imagery.

Table 2. Processing workflow with corresponding parameters in Metashape for generating Orthomosaic from UAS imagery.

Task	Parameter (NIR/RGB)
Align photos (Processing time for approximately 900 to 1400 images: 8 to 12 hrs)	Accuracy: Highest [2]/Medium [2] Pair selection: Reference [1] Key point limit: 60,000 [2] Tie point limit: 0 [2]
Optimize photo alignment (Adaptive camera model fit) (2 to 5 min)	Projection accuracy (pix): 0.1 [1] Tie point accuracy (pix): 0.3 [2] Fit: f, cx, cy, k1-4, p1-4 [1]
Build dense cloud (8 to 12 hrs)	Quality: Medium [2] Depth filtering: Aggressive [2]
Build mesh (1 to 2 hrs)	Surface type: Height field [1] Source data: Dense cloud [1] Face count: Medium [2] Interpolation: Enabled (default) [1]
Color calibration (varies as per number of images to be corrected in a block)	Source: Model [1] Calibrate white balance: Checked [1]
Build orthomosaic (8 to 10 hrs)	Projection type: Geographic [1] Surface: Mesh [1] Blending mode: Mosaic (default) [1] Enable hole filling: Checked [1]

[1]Parameters selected based on online tutorial; [2]Parameters selected using trial and error approach.

Images were aligned using the photo alignment process, involving tie point detection, selecting matching point pairs, and estimating improved camera coordinates. Metashape generates a point cloud as a 3D representation of tie-points. The highest alignment accuracy was used in conjuction with the original NIR image spatial resolution and the medium setting with the RGB images for tie point pair selection (Agisoft, 2017b). Being the first step in the workflow, Alignment setting plays an important role in estimating tie point positions, to accurately tie the images together. The key point limit was set to

60,000 and tie point limit was set to 0 to retain all matched points. A key point is a feature point with unique texture or high contrast found on multiple overlapping images. Using a higher key point value improves the chances for a successful alignment. A larger key point limit ensures more points are sampled by Metashape, potentially with a higher accuracy (Agisoft, 2017b). A tie point is a key point found on two or more images and used to optimize model performance. When using a tie point limit of 0, no prefiltering occurred, processing times were longer, but image correction was improved. Using the highest quality setting requires longer processing times, as it upscales the imagery by factor of 4 and helps acquire more accurate camera positions, is recommended for research purposes (Agisoft, 2017b).

The complex canopy structure of dense vegetation along with relief displacement made it extremely difficult to identify distinct spatial features between adjacent images and affected the geometric alignment between the photos. Medium alignment setting smooths the data with a 2x resampling and does not require accurate feature point location compared to high alignment, which uses the original spatial resolution of the photos (Agisoft, 2017b). Hence it was used to minimize the parallax and differing reflectance values to achieve additional calibrated images.

Optimization, using the adaptive camera model fit, includes a least squares bundle adjustment (Wolf et al., 2014), which estimates the internal and external camera orientation plus measurement parameters, estimating focal length (via exif data or user

input), if unknown, and corrects camera lens distortion. It is important to perform optimization in order to reduce the lens distortion effects on the forest structures in the photos (Agisoft, 2017b). After optimization, the standard error of unit weight (SEUW) value was between 0.1 and 0.3, below the recommended SEUW tolerance of 1.0.

A dense point cloud was derived from the images generated from the optimized camera parameters. Medium quality and aggressive depth filtering mode (Agisoft, 2022) were used for both the NIR and RGB imagery as reconstruction parameters. Metashape creates depth maps for each image. In order to remove the outliers and noise from the aerial imagery depth filtering was recommended by Agisoft (2017b) to use. We aligned the images with highest settings whereas dense cloud was generated at medium quality which might impact the elevation but does not impact the orthophoto as the amount of points generated are usually more than sufficient to generate the final orthoimage. Another important factor to consider was the computer memory as when we tried generating the dense cloud with high settings it ran out of memory and gave an error. To overcome the processing error, we applied the medium setting. Processing time for two blocks together was 8-10 hours.

3.2 Mesh Generation

Polygonal mesh generation created a 3D surface model based on the point cloud (dense or sparse). The height field option (which represents planar surfaces) was selected for the mesh generation. The height field is a surface type that represents topographic surface models. It requires lower amounts of memory to process large datasets (Agisoft, 2017b).

The dense cloud was used as the source data in processing though it requires longer processing time, it generates high quality result. Medium quality which produces little less detailed feature formations but help remove more noise or artifacts (Saczuk, 2018), was used for both NIR and RGB data polygon count generation; and, high settings were avoided as it can cause model visualization problem due to very high number count. Default interpolation setting and all point classes were used. Using interpolation helps the software interpolate surface areas around each dense cloud point by creating a circle of certain radius around them and fills some hole automatically (Agisoft, 2017b). The processing time was around 1-2 hours for two blocks.

3.3 Color Calibration

Portions of the RGB imagery exhibited vignetting; thus, color correction was applied to before orthomosaic was generated. Vignetting is defined as the reduction in an image's brightness towards the edge when compared with its center (Kim & Pollefeys, 2008). Vignetting arises due to the changes in irradiance over the image plane due to sensor geometry (Kelcey & Lucieer, 2012), and color correction balances the brightness variation across the imagery block (Agisoft, 2017b). As the data was acquired at various times of the day, changing illuminance was anticipated. If color calibration is not utilized, Metashape only blends images in overlapping areas, and does not change the brightness values (digital numbers) of the original images. The software's white balance option was used to correct each band independently. White balance adjusted the brightness values so

the image looks more “natural” by removing color casts. Calibrations times vary based on the number of images in a block.

3.4 ***Orthomosaic***

In the final stage of the process, an orthomosaic was generated using the mesh model for an elevation reference and blending along the photo’s seamlines. Pixel size was kept to default (i.e. image resolution, 1.3 cm for the NIR and 2.0 cm for the RGB). Hole filling option was kept on to remove any salt-and-pepper effects caused in part by shadows and to ensure there are no tiny gaps in the imagery. The software corrects image distortion followed by a multi-view stereo reconstruction procedure to place each pixel located in its correct XYZ position (Agisoft, 2017b).

The orthomosaic for each block was exported as a TIFF with no compression or tiling and reprojected to UTM NAD83 zone 16N (EPSG:26916) projected coordinate system. Dense points clouds were exported in ASPRS LAS format. The model was also exported as a KMZ file for use in Google Earth. Metadata documentation (PDF) for each block included all processing parameter specifications such as processing times for each segment, numbers of tie points, and number of dense cloud points, camera calibration information including point locations and errors, and orientation.

4. Results and Discussion

Metashape generated tie-points and orthomosaics with medium sized data gaps for the NIR data and large data gaps in the RGB data processing. With the NIR data, gaps occurred over water and dense forest areas. However, with RGB data, the low accuracy GNSS receiver quality on the UX5 potentially caused the data gaps due to poor quality initial estimation parameters. Collected image coordinates and orientation parameters were used for initial approximation in the photogrammetric processing. Higher accuracy GNSS enables much higher fidelity in the initial approximations, and the remaining image orientation, relative orientation, and block adjustment were calculated using photogrammetric aero-triangulation, which occurs in the image alignment and optimization steps. For both Ogontz and Wedens Bay (Figure 6 a; Figure 8 a, b), the software was able to generate tie-points for coastal areas. Large open areas made it easy for Metashape to generate tie-points in Sturgeon River Delta (Figure 7 b) and it was the only study site with no gaps in the RGB imagery.

Initially, only one block was processed at a time due to computer memory concerns. Later, multiple adjacent blocks were processed simultaneously, and in some cases, this increased the number of tie-points. Figure 5 shows the photogrammetric processing of three adjacent blocks aligned in Metashape. Figures 6, 7, and 8 show complete mosaicked NIR and RGB blocks. The mosaicking was completed using MosaicPro in ERDAS IMAGINE software (Hexagon, 2016), and proved efficient in generating seamless mosaics. Each flight block had different lighting condition due to varying acquisition

times during the day. This may impact additional digital image processing such as reduction of shadow effects by topographic normalization. This procedure may not be completed in a mosaic of all the blocks. Instead, topographic normalization would have to be performed in each block prior to creating the full mosaic. It should be noted that in many cases, image mosaics were better for classification when flown on days with cloud cover, due to fewer shadows, blurriness and glare.

All of the processed NIR blocks showed small data gaps, with the lowest number of gaps in the Sturgeon Delta and Wedens Bay (Figures 7a and 8a); whereas Ogontz Bay (Figure 6a) showed the highest amount of gap in the mosaicked imagery. The gaps visible in Wedens Bay NIR imagery were in areas not flown due to lack of a clear line of sight of the aircraft. The relief displacement of trees on large scale images, aircraft rotations caused by wind, the complex geometry of dense forested areas, and low oblique imagery, all contributed created problems for Metashape and other SfM software to find matching tie points, which led to huge gaps with the RGB imagery. In future studies we may increase the overlap to 90% by flying at higher elevations, if approved by the FAA. This would reduce the low oblique look angle and relief displacement. Final orthomosaics were generated at ground resolution of approximately 1.3 cm for the NIR and 2.0 cm spatial resolution for the RGB data.

It is important to experiment with the settings and options of photogrammetric software when processing such large amounts of data. For many of the NIR and RGB blocks, the

process was run using each available setting, (Low, Lowest, Medium, High, Highest and Ultra High) to ascertain which resulted in acceptable imagery quality and minimal data gaps in the block mosaics. For several cases, using the high settings for alignment created huge image gaps, while the medium settings did not. Performing realignment after the initial alignment process was crucial. Many blocks showed improved alignment on successive attempts. Metashape did process water areas close to beaches and vegetated areas if there were identifiable features in adjacent images such as underwater rocks, sand bars and emergent vegetation.

It has been observed when working with dense forest areas and acquiring a large digital dataset with lower accuracy GNSS, medium settings may work best for the alignment. Running the low setting during alignment might align a several more images in the blocks, but should be avoided as images are downscaled by factor of 16, leaving out important details (Agisoft, 2017b). Significant downscaling was evaluated but never achieved full image alignment.

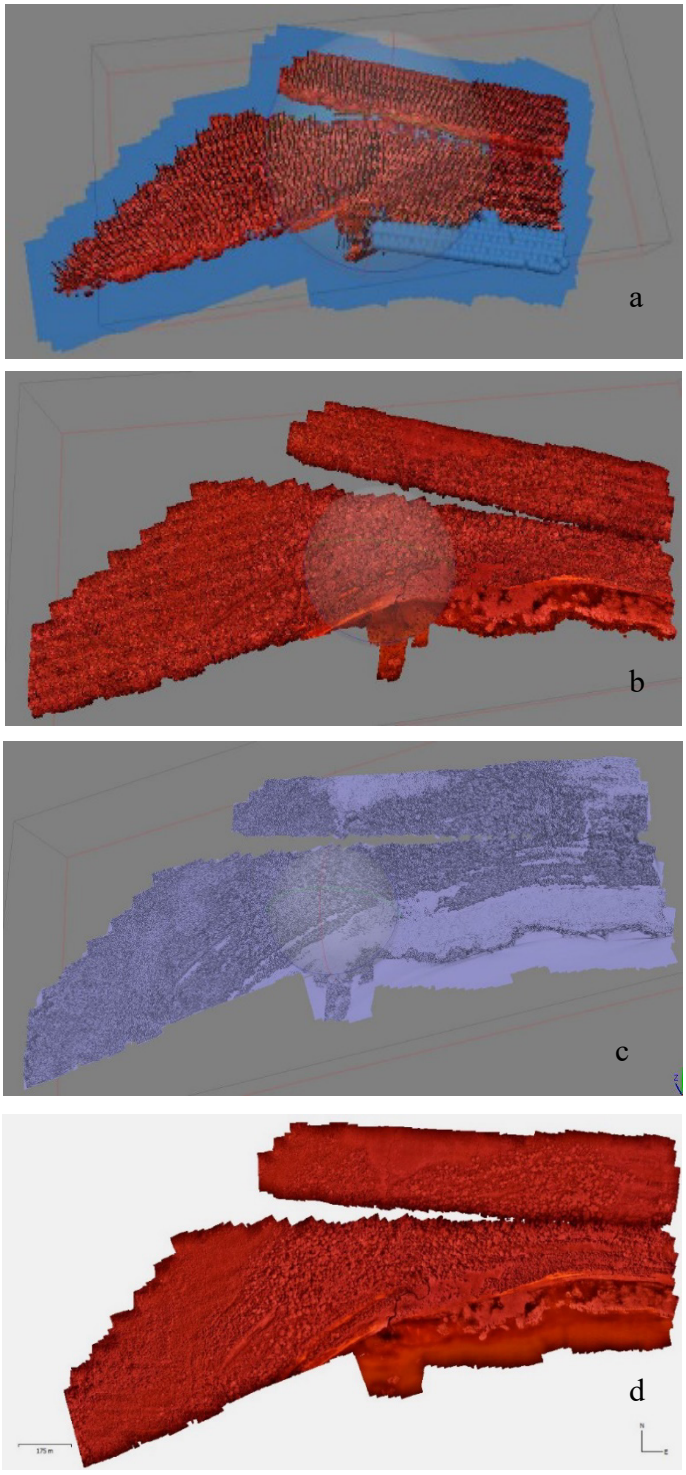

Figure 5. Tie points (a), dense cloud (b), 3D-Mesh (c), and orthomosaic (d) image generated from Metashape as part of photogrammetric workflow.

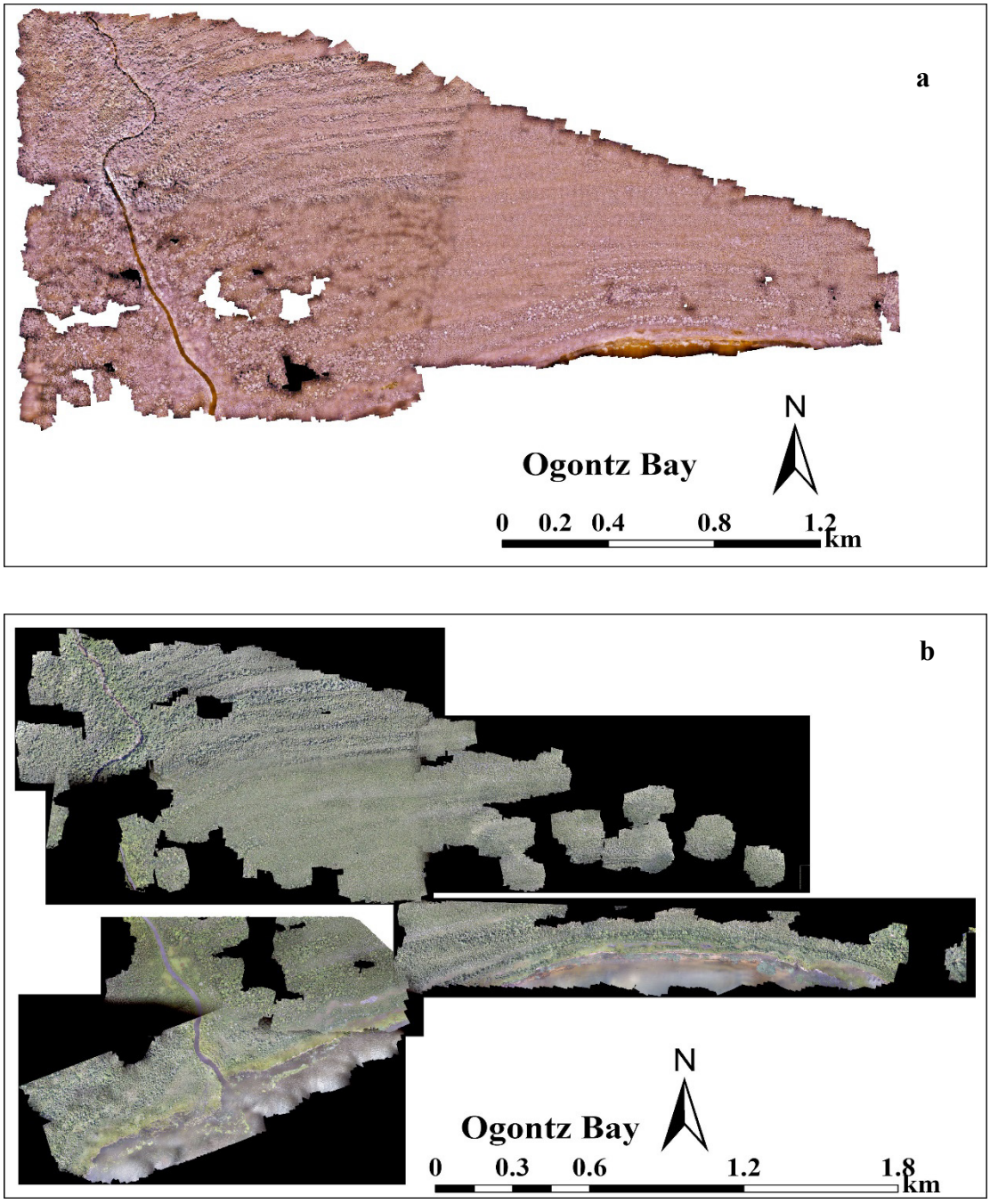

Figure 6. NIR (a) and RGB (b) mosaics of Ogontz Bay.

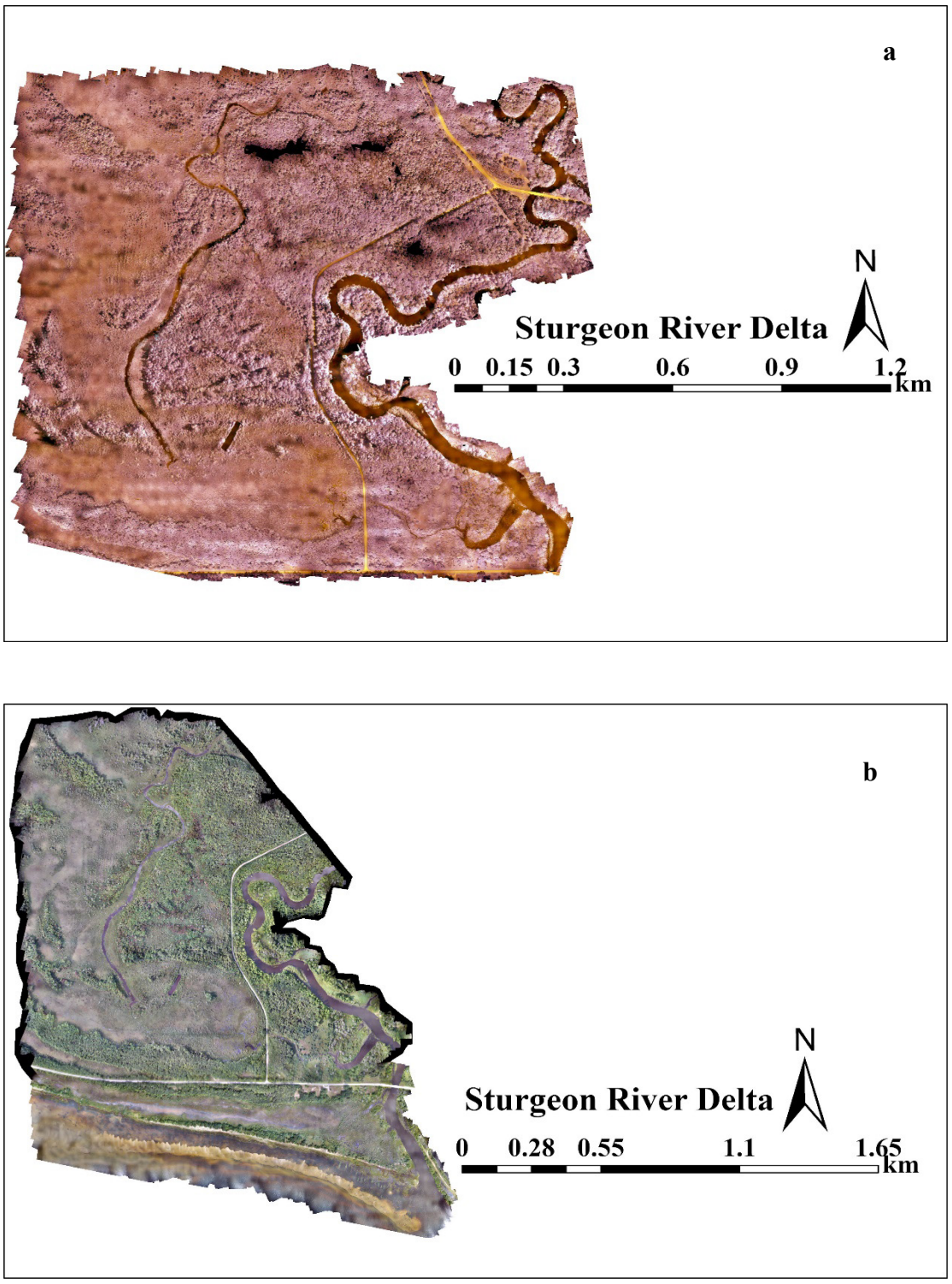

Figure 7. NIR (a) and RGB (b) mosaics of the Sturgeon River Delta.

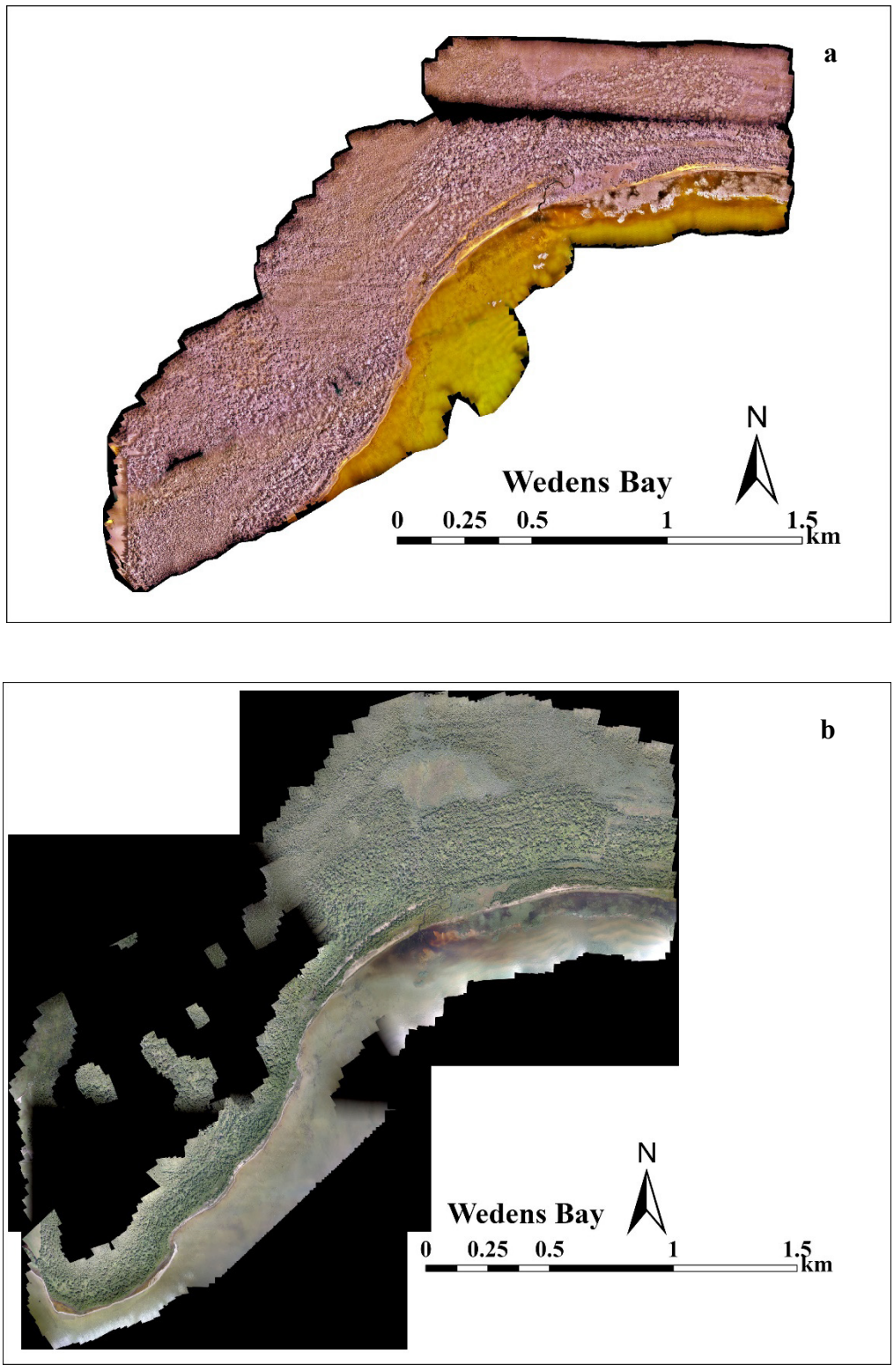

Figure 8. NIR (a) and RGB (b) mosaics of Wedens Bay.

With Metashape, higher accuracy requirements increased processing times which also depended on the complexity of the image texture. Due to the physical size of the raw data and the new data created with each processing, a large hard drive (5 to 8 terabytes) and adequate RAM were necessary. Thirty-five blocks, each having 800 to 1500 images, were processed for the three study sites. Each image was approximately 10 MB, consisting of 7,360 rows × 4,912 columns. The process was performed on a computer with 3.4 GHz CPU, Intel i5 processor using 64-bit Microsoft Windows 10 operating system with 16 GB of RAM (64 GB and GPU enabled PCs recommended for faster and larger data process). Increasing the computing capability enables processing the dataset for entire area at once, rather than individual blocks. It took 60 to 65 days to process the entire dataset. Cloud processing can be another option, but it's also time consuming and expensive.

5. Conclusion

The purpose of this applications paper was to discuss UAS image SfM photogrammetric workflow when working in a remote, dense forest environment, and acquiring large datasets with high spatial resolution image to create orthomosaics. This goal was achieved reasonably well. The methods described should help researchers and professionals to design and select an appropriate workflow.

The study demonstrated the flexibility of a UAS platform managed by a single person to collect data at different locations and times. Compared to human piloted aircraft platforms, UAS allows higher spatial resolution, cloud free data due to low altitude flying heights, pilot safety, minimum requirements for takeoff and landing, and cost savings.

High image overlap (80%) and use of a higher grade GNSS on the UAS (UX5-HP) helped achieve good quality orthoimages with NIR data; whereas with the RGB data SfM did not achieve the same quality due to lower grade GNSS on the UX5 UAS. A study by Dandois et al. (2015) showed that using high image overlap (>80%) in forested environment help achieve higher point cloud density. Higher flying heights covers more area as it provides a wider field of view, and may increase chances of matching identical features in homogenous forest and wetland cover imagery. In addition, the dense forest canopy negatively impacted image matching. Higher flying heights with increased image overlap as high as 90% is recommended. Higher flying heights help limit the amount of movement in the trees between image sets as the distance between the trees get smaller.

Any movement in-between the image-sets adds error in the geometry, thus reducing number of tie-points. Increasing the overlap does increase the chance of finding a greater number of tie-points but it comes with a trade-off, as it increases the uncertainty in vertical measurements affecting the accuracy of the elevation model.

Flying at higher altitude, with appropriate FAA waivers should improve image alignment due to the reduction in oblique viewing angles, and perpendicular flight lines should reduce image gaps. Current FAA regulation required the aircraft within the visual line of sight and remain below 122 m (400 ft) above ground level (AGL). A recent study done by Seifert et al. (2019) showed that higher overlap and flying altitudes impacts image reconstruction details and accuracy. All of the individually processed orthoimages were mosaicked into one single seamless mosaic for each study site. There were some variation in shadow and sunlight as the images were taken at different times throughout the day, from early morning to late afternoon with different camera settings. Therefore, certain image enhancement techniques, such as topographic normalization and histogram adjustments should be completed by block by block before creating the mosaics. It is also recommended that data acquisition take place in the months of July and August as an optimal season for mapping forest areas due to longer days and higher amount of sunlight. Wind speed variation, increased aircraft rotations (yaw, pitch and roll), and tree crowns movement caused blurred images in several blocks, but the 80% overlap used in this study help overcome some of the issues during processing.

We concluded UAS imagery coupled with the SfM and traditional photogrammetry technique offers great potential for future research in vegetation and wetland classification, identification and mapping at the species level, to observe shoreline changes. It is efficient and affordable providing imagery at reduced cost over manned aircraft. UAS systems can also be used with multispectral, hyperspectral, thermal, and LiDAR sensors (Sankey et al., 2017). UAS imageries are an efficient and affordable data at reduced cost over manned aircraft systems or high-resolution private satellites.

Funding: This research was funded by the USDA Forest Service, Agreement Number 17-PA-11091000-023 and by the College of Forest Resources and Environmental Sciences

Acknowledgments: The authors are grateful to the USDA Forest Service for the funding of this project. We are grateful to Jim Ozenberger, Hiawatha National Forest for his advice and recommendations. Particular thanks to Jeff L. Sloan and Mark Bauer at the National Unmanned Aircraft Systems Project Office, USGS and to Gordon Maclean for his wetlands mapping expertise.

Document references

Agisoft. L. 2017a. AgiSoft PhotoScan Professional (Version 1.3.0) (Software). URL: http://www.agisoft.com/downloads/installer/.

Agisoft. L. 2017b. Photoscan User Manual: Professional Edition, Version 1.3. URL: https://www.agisoft.com/downloads/user-manuals/.

CAA. 2015. An introduction to unmanned aircraft systems. URL: https://www.caa.co.uk/Consumers/Unmanned-aircraft/Our-role/An-introduction-to-unmanned-aircraft-systems/ (last date accessed: 21 November 2019).

DoD. U.S.D.o.D. 2019. UNMANNED AIRCRAFT SYSTEMS (UAS). URL: https://dod.defense.gov/UAS/ (last date accessed: 21 November 2019).

FAA. 2018. Small Unmanned Aircraft Regulations (Part 107). URL: https://www.faa.gov/news/fact_sheets/news_story.cfm?newsId=22615 (last date accessed: 21 November 2019).

Hexagon. G. 2016. ERDAS IMAGINE (Version 16.00) (64-bit). URL: https://download.hexagongeospatial.com/downloads/imagine/erdas-imagine-2016-64-bit (last date accessed: 21 November 2019).

ICAO. 2011. UAS Documents / Cir 328 AN/190 Unmanned Aircraft Systems (UAS). URL: https://www.icao.int/Meetings/UAS/Pages/UAS_Documents.aspx (last date accessed: 21 November 2019).

Markets. 2018. Unmanned Aerial Vehicle (UAV) Market by Application (ISR, Precision Agriculture, Product Delivery), Class (Tactical, MALE, HALE, UCAV), System (Avionics, Sensors, Payload), MTOW (<25Kg, 25-150Kg, >150kg), Range, Type, and Region - Global Forecast to 2025. URL: https://www.marketsandmarkets.com/Market-Reports/unmanned-aerial-vehicles-uav-market-662.html (last date accessed: 21 November 2019).

NASA. 2017. Mini-Sniffer. URL: https://www.nasa.gov/centers/dryden/multimedia/imagegallery/Mini-Sniffer/Mini-Sniffer_proj_desc.html (last date accessed: 21 November 2019).

NASA. 2008. The Promise of ERAST: Dryden Flight Research Center. URL: https://www.nasa.gov/centers/dryden/news/X-Press/stories/102904_people_erast.html (last date accessed: 21 November 2019).

Saczuk, E. (2018). –3-D Mesh Surface. *Processing UAS Photogrammetric Images in Agisoft Photoscan Professional.*

Trimble. 2019a. Trimble Inpho UASMaster. URL: https://geospatial.trimble.com/products-and-solutions/trimble-inpho-uasmaster (last date accessed: 5 November 2019).

Trimble, 2019b. Trimble UX5 Aerial Imaging Solution for Agriculture. URL: https://www.trimble.com/agriculture/ux5 (last date accessed: 5 November 2019).

References Cited

Adam, E., Mutanga, O., & Rugege, D. (2009). Multispectral and hyperspectral remote sensing for identification and mapping of wetland vegetation: a review. *Wetlands Ecology and Management, 18*(3), 281-296. doi:10.1007/s11273-009-9169-z

Agisoft, L. (2022). Metashape User Manual: Professional Edition, Version 1.8. Retrieved from https://www.agisoft.com/downloads/user-manuals/

Bai, Y., Mas, E., & Koshimura, S. (2018). Towards operational satellite-based damage-mapping using u-net convolutional network: A case study of 2011 tohoku earthquake-tsunami. *Remote Sensing, 10*(10), 1626.

Bendig, J., Bolten, A., Bennertz, S., Broscheit, J., Eichfuss, S., & Bareth, G. (2014). Estimating Biomass of Barley Using Crop Surface Models (CSMs) Derived from UAV-Based RGB Imaging. *Remote Sensing, 6*(11), 10395-10412. doi:10.3390/rs61110395

Berhane, T. M., Lane, C. R., Wu, Q., Autrey, B. C., Anenkhonov, O. A., Chepinoga, V. V., & Liu, H. (2018). Decision-Tree, Rule-Based, and Random Forest Classification of High-Resolution Multispectral Imagery for Wetland Mapping and Inventory. *Remote Sens (Basel), 10*(4), 580. doi:10.3390/rs10040580

Bhatt, P. (2018). *Mapping Coastal Wetland and Phragmites on the Hiawatha National Forest Using Unmanned Aerial System (UAS) Imagery: Proof of Concepts.* Michigan Technological University,

Bhatt, P., Maclean, A., Dickinson, Y., & Kumar, C. (2022). Fine-Scale Mapping of Natural Ecological Communities Using Machine Learning Approaches. *Remote Sensing, 14*(3), 563.

Boon, M. A., Drijfhout, A. P., & Tesfamichael, S. (2017). Comparison of a Fixed-Wing and Multi-Rotor Uav for Environmental Mapping Applications: A Case Study. *ISPRS - International Archives of the Photogrammetry, Remote Sensing and Spatial Information Sciences, XLII-2/W6*, 47-54. doi:10.5194/isprs-archives-XLII-2-W6-47-2017

Cai, G., Dias, J., & Seneviratne, L. (2014). A survey of small-scale unmanned aerial vehicles: Recent advances and future development trends. *Unmanned Systems, 2*(02), 175-199.

Carbonneau, P. E., & Dietrich, J. T. (2017). Cost-effective non-metric photogrammetry from consumer-grade sUAS: implications for direct georeferencing of structure from motion photogrammetry. *Earth Surface Processes and Landforms, 42*(3), 473-486. doi:10.1002/esp.4012

Casana, J., & Panahipour, M. (2014). Satellite-based monitoring of looting and damage to archaeological sites in Syria. *Journal of Eastern Mediterranean Archaeology & Heritage Studies, 2*(2), 128-151.

Chiang, K. W., Tsai, M. L., & Chu, C. H. (2012). The development of an UAV borne direct georeferenced photogrammetric platform for Ground Control Point free applications. *Sensors (Basel), 12*(7), 9161-9180. doi:10.3390/s120709161

Colomina, I., & Molina, P. (2014). Unmanned aerial systems for photogrammetry and remote sensing: A review. *ISPRS Journal of Photogrammetry and Remote Sensing, 92*, 79-97. doi:10.1016/j.isprsjprs.2014.02.013

Dandois, J., Olano, M., & Ellis, E. (2015). Optimal Altitude, Overlap, and Weather Conditions for Computer Vision UAV Estimates of Forest Structure. *Remote Sensing, 7*(10), 13895-13920. doi:10.3390/rs71013895

Dandois, J. P., & Ellis, E. C. (2013). High spatial resolution three-dimensional mapping of vegetation spectral dynamics using computer vision. *Remote Sensing of Environment, 136*, 259-276.

Dunford, R., Michel, K., Gagnage, M., Piégay, H., & Trémelo, M. L. (2009). Potential and constraints of Unmanned Aerial Vehicle technology for the characterization of Mediterranean riparian forest. *International Journal of Remote Sensing, 30*(19), 4915-4935. doi:10.1080/01431160903023025

Eling, C., Wieland, M., Hess, C., Klingbeil, L., & Kuhlmann, H. (2015). Development and Evaluation of a Uav Based Mapping System for Remote Sensing and Surveying Applications. *ISPRS - International Archives of the Photogrammetry, Remote Sensing and Spatial Information Sciences, XL-1/W4*, 233-239. doi:10.5194/isprsarchives-XL-1-W4-233-2015

Gabrlik, P. (2015). The use of direct georeferencing in aerial photogrammetry with micro UAV. *IFAC-PapersOnLine, 48*(4), 380-385.

Getzin, S., Wiegand, K., & Schöning, I. (2012). Assessing biodiversity in forests using very high-resolution images and unmanned aerial vehicles. *Methods in Ecology and Evolution, 3*(2), 397-404. doi:10.1111/j.2041-210X.2011.00158.x

Gini, R., Passoni, D., Pinto, L., & Sona, G. (2017). Use of Unmanned Aerial Systems for multispectral survey and tree classification: a test in a park area of northern Italy. *European Journal of Remote Sensing, 47*(1), 251-269. doi:10.5721/EuJRS20144716

Goodbody, T. R. H., Coops, N. C., Marshall, P. L., Tompalski, P., & Crawford, P. (2017). Unmanned aerial systems for precision forest inventory purposes: A review and case study. *The Forestry Chronicle, 93*(01), 71-81. doi:10.5558/tfc2017-012

Hayes, M. M., Miller, S. N., & Murphy, M. A. (2014). High-resolution landcover classification using Random Forest. *Remote sensing letters, 5*(2), 112-121.

Husson, E., Hagner, O., Ecke, F., & Schmidtlein, S. (2014). Unmanned aircraft systems help to map aquatic vegetation. *Applied Vegetation Science, 17*(3), 567-577. doi:10.1111/avsc.12072

Kelcey, J., & Lucieer, A. (2012). Sensor Correction of a 6-Band Multispectral Imaging Sensor for UAV Remote Sensing. *Remote Sensing, 4*(5), 1462-1493. Retrieved from https://www.mdpi.com/2072-4292/4/5/1462

Kim, S. J., & Pollefeys, M. (2008). Robust radiometric calibration and vignetting correction. *IEEE Trans Pattern Anal Mach Intell, 30*(4), 562-576. doi:10.1109/TPAMI.2007.70732

Koh, L. P., & Wich, S. A. (2012). Dawn of Drone Ecology: Low-Cost Autonomous Aerial Vehicles for Conservation. *Tropical Conservation Science, 5*(2), 121-132. doi:10.1177/194008291200500202

Mian, O., Lutes, J., Lipa, G., Hutton, J. J., Gavelle, E., & Borghini, S. (2015). Direct Georeferencing on Small Unmanned Aerial Platforms for Improved Reliability and Accuracy of Mapping without the Need for Ground Control Points. *ISPRS - International Archives of the Photogrammetry, Remote Sensing and Spatial Information Sciences, XL-1/W4*, 397-402. doi:10.5194/isprsarchives-XL-1-W4-397-2015

Rango, A., Laliberte, A., Herrick, J. E., Winters, C., Havstad, K., Steele, C., & Browning, D. (2009). *Unmanned aerial vehicle-based remote sensing for rangeland assessment, monitoring, and management* (Vol. 3): SPIE.

Samiappan, S., Turnage, G., Hathcock, L., Casagrande, L., Stinson, P., & Moorhead, R. (2016). Using unmanned aerial vehicles for high-resolution remote sensing to map invasive Phragmites australis in coastal wetlands. *International Journal of Remote Sensing, 38*(8-10), 2199-2217. doi:10.1080/01431161.2016.1239288

Samiappan, S., Turnage, G., Hathcock, L. A., & Moorhead, R. (2016). Mapping of invasive phragmites (common reed) in Gulf of Mexico coastal wetlands using multispectral imagery

and small unmanned aerial systems. *International Journal of Remote Sensing, 38*(8-10), 2861-2882. doi:10.1080/01431161.2016.1271480

Sankey, T., Donager, J., McVay, J., & Sankey, J. B. (2017). UAV lidar and hyperspectral fusion for forest monitoring in the southwestern USA. *Remote Sensing of Environment, 195*, 30-43. doi:10.1016/j.rse.2017.04.007

Seifert, E., Seifert, S., Vogt, H., Drew, D., van Aardt, J., Kunneke, A., & Seifert, T. (2019). Influence of Drone Altitude, Image Overlap, and Optical Sensor Resolution on Multi-View Reconstruction of Forest Images. *Remote Sensing, 11*(10). doi:10.3390/rs11101252

Sidike, P., Sagan, V., Maimaitijiang, M., Maimaitiyiming, M., Shakoor, N., Burken, J., . . . Fritschi, F. B. (2019). dPEN: Deep Progressively Expanded Network for mapping heterogeneous agricultural landscape using WorldView-3 satellite imagery. *Remote Sensing of Environment, 221*, 756-772.

Sloan, J. L. (2017). [National Unmanned Aircraft Systems Project Office: U.S. Geological Survey, Agisoft PhotoScan Workflow].

Thamm, F. P., Brieger, N., Neitzke, K. P., Meyer, M., Jansen, R., & Mönninghof, M. (2015). SONGBIRD – AN INNOVATIVE UAS COMBINING THE ADVANTAGES OF FIXED WING AND MULTI ROTOR UAS. *ISPRS - International Archives of the Photogrammetry, Remote Sensing and Spatial Information Sciences, XL-1/W4*, 345-349. doi:10.5194/isprsarchives-XL-1-W4-345-2015

Torresan, C., Berton, A., Carotenuto, F., Di Gennaro, S. F., Gioli, B., Matese, A., . . . Wallace, L. (2016). Forestry applications of UAVs in Europe: a review. *International Journal of Remote Sensing, 38*(8-10), 2427-2447. doi:10.1080/01431161.2016.1252477

Turner, D., Lucieer, A., & Wallace, L. (2014). Direct Georeferencing of Ultrahigh-Resolution UAV Imagery. *IEEE Transactions on Geoscience and Remote Sensing, 52*(5), 2738-2745. doi:10.1109/tgrs.2013.2265295

US Forest Service, U. F. S. (2015). Land Areas Report (LAR): Table 4 – Areas by State. Retrieved from https://www.fs.fed.us/land/staff/lar/LAR2015/lar2015index.html

Watts, A. C., Ambrosia, V. G., & Hinkley, E. A. (2012). Unmanned Aircraft Systems in Remote Sensing and Scientific Research: Classification and Considerations of Use. *Remote Sensing, 4*(6), 1671-1692. doi:10.3390/rs4061671

Wolf, P. R., Dewitt, B. A., & Wilkinson, B. E. (2014). *Elements of Photogrammetry with Applications in GIS*: McGraw-Hill Education.